Eliminating micro-porous layer from gas diffusion electrode for use in high temperature polymer electrolyte membrane fuel cell

Huaneng Su [a], Qian Xu [a,*], Junjie Chong [b], Huaming Li [a], Cordellia Sita [b], Sivakumar Pasupathi [b]

[a] *Institute for Energy Research, Jiangsu University, 301 Xuefu Road, Zhenjiang 212013, PR China*

[b] *South African Institute for Advanced Materials Chemistry, University of the Western Cape, Private Bag X17, Bellville 7535, South Africa*

*Corresponding author. Tel: +86-511-88799500; Fax: +86-511-88799500; E-mail address: suhuaneng@gmail.com

Abstract

In this work, we report a simple strategy to improve the performance of high temperature polymer electrolyte membrane fuel cell (HT-PEMFC) by eliminating the micro-porous layer (MPL) from its gas diffusion electrodes (GDEs). Due to the absence of liquid water and the general use of high amount of catalyst, the MPL in a HT-PEMFC system works limitedly. Contrarily, the elimination of the MPL leads to an interlaced micropore/macropore composited structure in the catalyst layer (CL), which favors gas transport and catalyst utilization, resulting in a greatly improved single cell performance. At the normal working voltage (0.6 V), the current density of the GDE eliminated MPL reaches 0.29 A cm^{-2}, and a maximum power density of 0.54 W cm^{-2} at 0.36 V is obtained, which are comparable to the best results yet reported for the HT-PEMFCs with similar Pt loading and operated using air. Furthermore, the MPL-free GDE maintains an excellent durability during a preliminary 1,400 hour HT-PEMFC operation, owing to its structure advantages, indicating the feasibility of this electrode for practical applications.

Keywords: High temperature polymer electrolyte membrane fuel cell; Membrane electrode assembly; Gas diffusion electrode; Micro-porous layer; Catalyst layer

1. Introduction

Operating polymer electrolyte membrane fuel cells (PEMFCs) at high temperature (120 ^{o}C-200 ^{o}C) can avoid some intrinsic challenges they faced at low temperature, such as complex humidification and heat management, low resistance to CO catalyst poisoning and potentially high technology costs [1]. For two decades, polybenzimidazole membranes (PBI, or its derivatives) doped with phosphoric acid (PA), which can serve as proton exchange membranes for PEMFCs, have always been considered as the best candidates for high temperature operation [2]. This type of HT-PEMFCs can normally operate between 150 ^{o}C -200 ^{o}C, offering merits like high CO tolerance, simplified water/thermal management, which are seen as critical advantages in vehicle applications [3-6]. However, the performances of these HT-PEMFCs, even with high catalyst loadings, are still inferior to the conventional LT-PEMFCs based on Nafion membranes. For one of the reasons it lies in the presence of PA, which impedes the transport of reactant gases from the support layers to the catalyst active sites, resulting in high mass transfer resistance, consequently slow electrodes reaction processes [7,8]. To enhance the performance, one of the promising solutions is modifying the structure of the electrodes to enable them dealing with the electrochemical processes more efficiently [9,10].

At present, almost all electrodes for HT-PEMFCs were prepared as gas diffusion electrode (GDE) form, i.e., the supporting layer for the catalyst layer depositing is the

gas diffusion layer (GDL) instead of the membrane. Therefore, for HT-PEMFC the preparation of GDE is very important as it is the only place where electrochemical reactions occur, for which a decent inner structure should be established for smoothly transporting the reactant gases/produced water to/from the CL [11,12]. Normally, the GDE was structured with three layers, as illustrated in Fig. 1(a), i.e., CL, micro-porous layer (MPL) and gas diffusion backing layer (GDBL), in which MPL and GDBL are often joined together under the term GDL. The MPL is normally a layer of carbon powder bonded by certain amount of hydrophobic agent like polytetrafluoroethylene (PTFE). For a LT-PEMFC system, the role of MPL is very important due to its strong relevance to the water management. In LT-PEMFC systems, the pores in the CLs tends to be blocked due to the presence of liquid water, which are known as water flooding and it significantly affects the cell performance due to the high mass transfer resistance resulting from it. It is believed that the excess liquid water in the fuel cell system can be effectively removed by the MPL duo to the capillary effect resulting from its abundant micro pores. Therefore, the optimization of the MPL for LT-PEMFC systems has always attracted great attentions in both theoretical modeling and experimental studies [13-29].

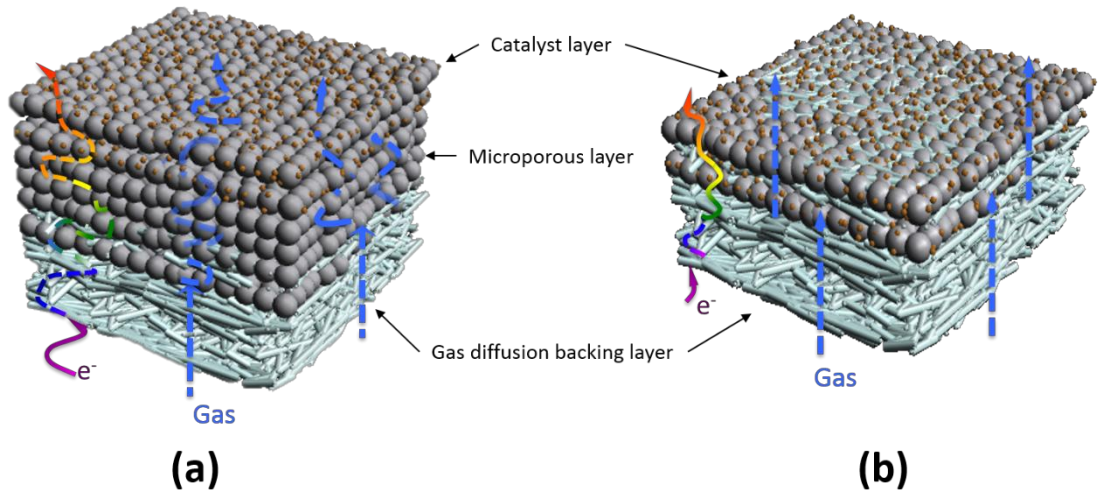

Fig. 1. Conceptual diagrams of the conventional GDE with MPL (a) and the GDE eliminated MPL (b).

However, only few works on MPL study [30,31] were found in HT-PEMFC field because the role of MPL in a HT-PEMFC system is limited because there exist no liquid water. HT-PEMFCs are generally operated at 120-200 ^{o}C where water exist as vapour, which makes the water removal much easier than that in LT-PEMFCs. Based on this reason, we speculate that HT-PEMFC GDEs can be structured with elimination of MPL, as illustrated in Fig. 1(b). Several advantages are expected from this structure: (i) enhanced gas permeability. Compared with the GDBL, whose mean pore size is in the range of 10-100 μm, the MPL features a finer pore structure with the pore size only several microns. The increase of micro-porosity can impede the gas flow, therefore the presence of MPL could decrease the gas permeability [31], (ii) decreased ohmic resistance. Though the presence of MPL can improve the interfacial contact between the supporting layer and the CL due to its flat and even surface, the inferior contact between the MPL and the uneven GDBL and the resistance of the

MPL itself should not be neglected. Therefore, for a MPL-free GDE in which the CL may also get inferior contact with GDBL, the resistance of the MPL itself at least does not exist, (iii) reduced cost and manpower. The deposition of MPL is time-consuming and laborious, several procedures are required including ink preparation, spraying and sintering, etc. The elimination of MPL, consequently, is economical and efficient.

Despite these advantages from eliminating MPL, the lack of MPL could increase the penetration of catalyst particles into the GDBL, resulting in reduced catalyst utilization. However, it is believed that GDBL with high content of polymerized PTFE (normally 20 wt.% − 30 wt.%) can effectively reduce the penetration of carbon/catalyst particles due to the polymer networks formed by sintering [32,33]. On the other hand, the Pt loadings used in PBI-based HT-PEMFC electrodes are generally as high as 0.7 mg cm^{-2} [34], which is much more than that in LT-PEMFCs, due to the high ORR Tafel slope in PA along with the anion adsorption of H_3PO_4 on Pt [35,36]. Therefore, it is speculated that the limited penetration of catalyst particles should has no serious effect on the catalyst utilization. For the first time in this work, we demonstrated the use of the GDEs eliminated MPL for HT-PEMFC showing high performance.

2. Experimental

2.1. Preparation of GDEs

The GDEs in this work were prepared using an automatic ultrasonic-spray coating technique [37,38], by which good homogeneity and reproducibility of the CLs as prepared were secured. Commercial 40 wt.% Pt/C catalyst (Hispec 4000, Johnson Matthey) was used for all GDEs. The catalyst ink for ultrasonic-spray coating was obtained by evenly mixing the catalyst powder, certain amount of PTFE suspension (60 wt.%, Aldrich) and the solvent isopropanol. A raw carbon paper (TGP-H-060, Toray, Japan) was used to prepare the GDBL for all electrodes. Before being used for MPL/CL deposition, the carbon paper was hydrophobically treated with certain concentration of Teflon dispersion, then calcined at 350 ^{o}C for 30 min to form an even PTFE network (~25 wt.% PTFE in the GDBL), which is believed to be effective on blocking the penetration of carbon powder/catalyst particles during MPL/CL preparation [32,33]. To prepare GDE without MPL, the catalyst ink was directly sprayed onto the surface of the GDBL to form the CL (Fig. 1(b)). For comparison, conventional GDEs with MPL were prepared. First, a slurry consisted of carbon powder (~85 wt.%) and Teflon (~15 wt.%) was deposited onto the GDBL to form MPL, then the CL was prepared onto the surface of the MPL (Fig. 1(a)) as same procedures for the MPL-free GDE.

After CL deposition, all GDEs were sintered in N_2 atmosphere for 20-30 min at 350 ^{o}C to further homogenize the polymerized PTFE network in each layer and to stabilize the whole GDE structure. The Pt loadings and the PTFE contents in the CLs of all GDEs were controlled at ~ 0.7 mg cm^{-2} and ~0.6 mg cm^{-2} respectively.

2.2. Physical characterization of the GDEs

The surface and section morphologies of the GDEs/MEAs were characterized by a field-emission SEM (Zeiss, Oberkochen, Germany). The determination of pore size distribution and porosity was conducted at Auto Pore IV 9500 Hg porometer (Micromeritics Instrument Corporation, USA).

2.3. Single cell test and electrochemical measurements

The instruments and procedures for single cell test and electrochemical measurements are same as described in our previous works [9]. In brief, the membrane electrode assemblies (MEAs) were made with the GDEs and ABPBI (poly(2,5-benzimidazole) membranes (Fumapem AM, FuMA-Tech, Germany). For doping with PA, the membranes were immersed in 85% acid solution for certain time at 120 ^{o}C until their acid doping level of about 3.8 molecules of H_3PO_4 per polymer repeating unit (PRU) were obtained. For single cell and electrochemical impedance spectroscopy (EIS) tests, dry H_2 /Air (or O_2) were supplied with the stoichiometries of 1.5/2 at cell temperature 160 ^{o}C. The flow rate equivalent to 0.2 A cm^{-2} was used for current densities lower than 0.2 A cm^{-2}. Both the anode and cathode outlet were ambient pressure. Then the MEAs were assembled in a single cell fixture with an active area about 5 cm^2. Prior to the recording of the polarization curves, the MEAs were operated at constant load at 0.2 A cm^{-2} overnight for activation. The current-voltage polarization curves were obtained by measuring the voltage with two stepwise increments of current density.

The first and second section stepwise from 0 to 0.2 A cm^{-2} and 0.2 to 2 A cm^{-2} with an interval of 0.01 A cm^{-2} and 0.1 A cm^{-2}, respectively. At each current, the cell voltage was measured after a hold time of 5 min to allow the cell approaching steady state.

For cyclic voltammetry (CV) measurements, the feeding gas (Air or O_2) in cathode side was changed to dry N_2. More details on the tests and data processing can be found in our previous publications [9].

3. Results and discussion

3.1 Structure characterization

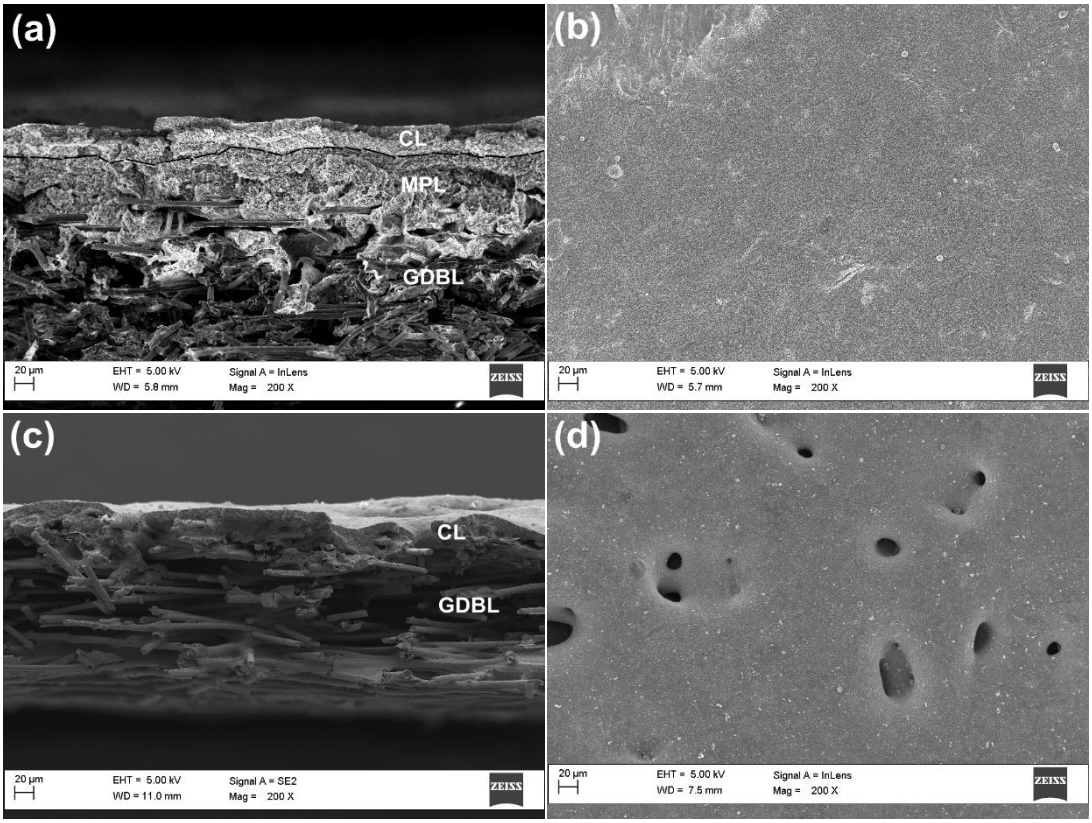

Fig. 2. SEM images of the GDE with MPL (a, b) and the GDE without MPL (c, d) to show their cross-sections and surface morphologies.

The differences in CL architecture and surface morphology between the two GDEs are shown in Fig. 2. By inspecting the cross-section images, it is clear the conventional GDE is much thicker due to the existence of MPL whose thickness is about 4-5 times that of the CL (see Fig. 2(a)), which means the increased gas transport resistance as the gases have to diffuse across the thick MPLs to access the CLs. In contrast, a CL/GDBL composited structure is observed form the MPL-free GDE (Fig. 2(c)) where the CL is mostly integrated into the macroporous structure of the GDBL.

And the CL were mainly concentrated in the surface layer of the GDBL, which suggests that no serious catalyst penetration occurred during the GDE preparation process, high catalyst utilization rate is then expected with the elimination of MPL. This is further confirmed by the cyclic voltammetry tests as shown in Fig. 3, where the two GDEs show similar electrochemical surface area (ECSA), implying that no serious catalyst loss due to penetration.

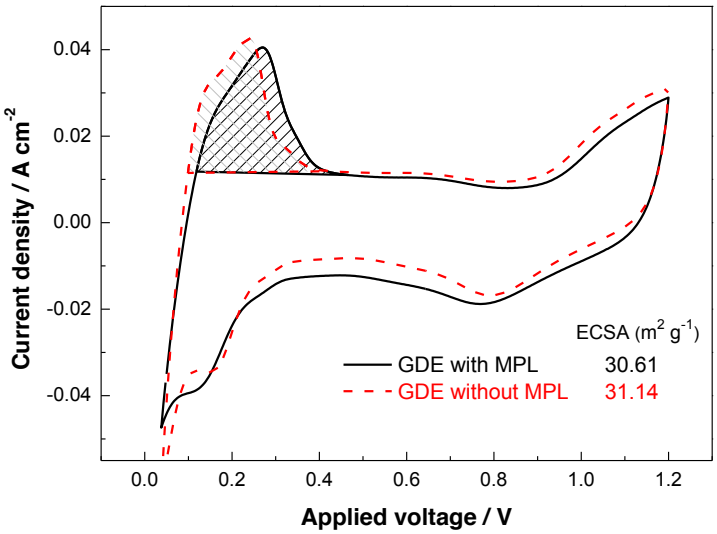

Fig. 3. Cyclic voltammograms of the MEAs with the different GDEs.

From the surface morphology image (Fig. 2(d)), it can be seen that a complete CL is still established on the surface of the GDBL. The catalyst particles are mainly deposited onto the stems and the junctions of the carbon fibers, adequate macroporos with diameters of about 20~30 μm, which originate from the GDBL, are still remained in the CL, resulting in an interlaced micropore/macropore composited CL structure that favors the gas transport and utilization as the catalyst particles around

the macropores are more accessible to the gases. Therefore, the catalyst active sites that participated in electrode reactions (e.g. ORR) at the Pt surface could be well spread in the whole CL than those in the normal GDEs, which suggests that the MPL-free GDE could possess higher output than the conventional one even their ECSAs are nearly same, because the latter shows a dense CL structure (Fig. 2(b)) that is solely dominated by microporos, which could lead to an inferior gas diffusion efficiency as the gases molecules tend to be impeded by fine carbon powder particles and the numerous micro-pore walls [39,40]. One concern from the surface morphology of the MPL-free GDE is its interface contact with the ABPBI membrane considering its uneven and macropore-rich surface, which could lead to an indecent contact and an inferior proton transport between the CL and the membrane. However, it does not seem to be a problem seen from the single cell test results showed later. We believe that a satisfactory interfacial contact can still be established due to the assembly pressure applied onto the GDEs in the single cell, along with the pliability of the acid-doped membranes, which is confirmed by the SEM examination on the tested MEA with the MPL-free GDEs shown later (see Fig. 6, Section 3.2). And the proton transfer in the electrodes depends on the "free PA" but not the membrane, therefore good proton transport can be maintained since the "free-PA" was pre-impregnated into the CL and mainly distributed within the micropores between the catalyst particles due to the capillary effect. We believe this CL configuration (i.e. interlaced micropore/macropore composited structure) could make more catalyst particles simultaneously accessible to both reactant gas and proton conductor (i.e. PA),

eventually leading to an improved cell performance.

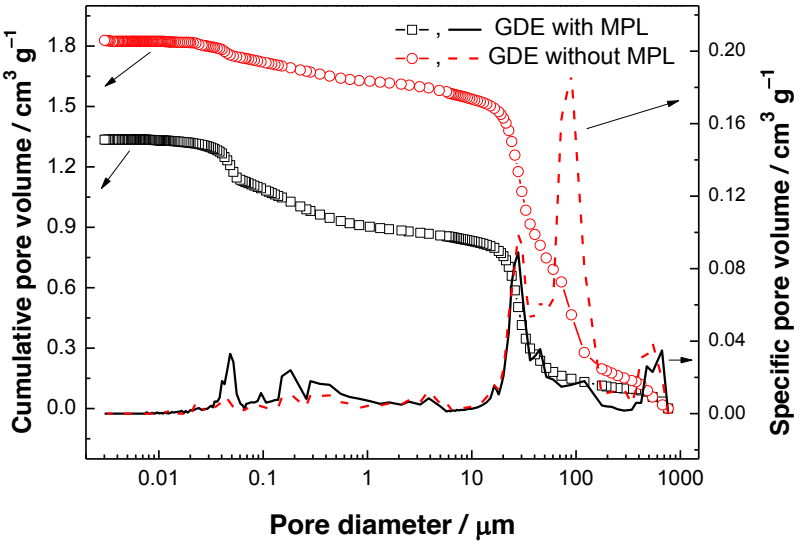

Fig. 4. Pore size distribution of the two GDEs.

The structural differences between the two GDEs are further demonstrated by pore sizes characterization using mercury intrusion method, as shown in Fig. 4. It shows that the elimination of MPL reduces the volume of micropores (0.03-0.1 um) and mesopores (0.1-2 um), however it greatly increased the volume of macropores in the range of 20~200 um, which leads to a substantial increase in cumulative pore volume (~37% higher than that of the conventional GDE, see Table 1). Due to the absences of liquid water during HT-PEMFC operation, the GDE with larger volume of the macropores is expected to deliver better mass transport due to the molecular diffusion mechanism [41]. The porosities of the two GDEs obtained from the mercury intrusion are also list in Table 1 for comparison. An increase of ~31% in porosity is also observed for the MPL-free GDE compared to the conventional one due to the great

increase in its macropore volumes. From the view of effective porosity, which is seen as a more practical structure parameter than the total porosity as it only reflects the pore spaces interconnected with each other and open to the surface [40], the MPL-free GDE should also has higher effective porosity owing to its 3D-interlaced micropore/macropore CL structure that makes more micropores between the catalyst particles open to or interconnected to the surfaces of the macropores within the CL. Theoretically, the operating current of the fuel cell relies on the gas diffusional flux [40]. It is anticipated that the MPL-free GDE possesses larger gas diffusional flux due to the much thinner diffusion layer and the higher effective porosity. Then, an achievement in elevating both fuel cell operating current and limiting current on the MPL-free GDE is expected, which is confirmed by the single cell tests showed below.

3.2 Single cell test

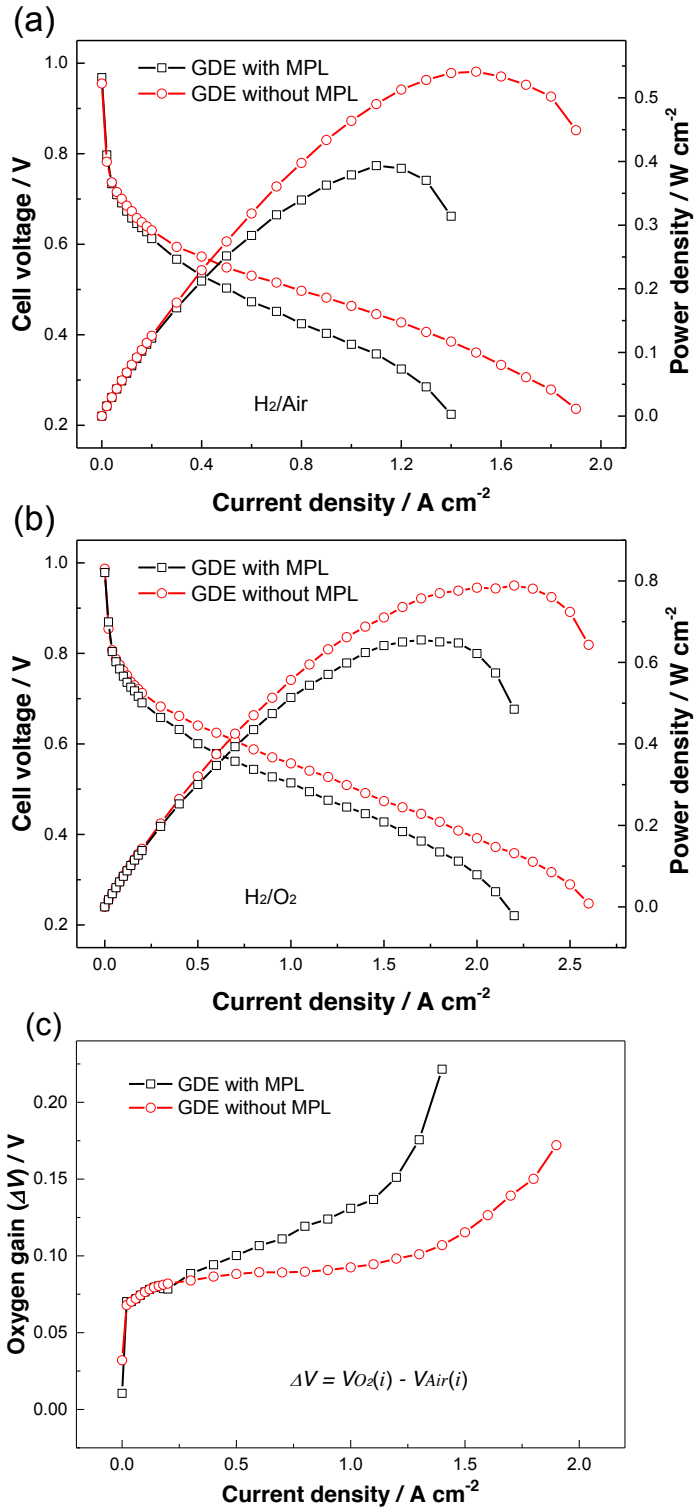

Fig. 5. Polarization curves and power density curves of the single cell using GDEs with/without MPL, operated at 160 ^{o}C and ambient pressure, with (a) 1.5/2 stoichiometry of H_2/Air, (b) 1.5/2 stoichiometry of H_2/O_2; and (c) Oxygen gain.

Fig. 5 exhibits the results of single cell operation with the different GDEs and different oxidants (Air or O_2). The polarization and power density curves of the two GDEs (with/without MPL) operating with H_2/Air are shown in Fig. 5(a). In low current density region (< 0.2 A cm^{-2}), the performance difference between the two GDEs is not significant because their performances are in the charge transfer-controlled region. However, this difference becomes prominent at high current densities (lower potential region) due to the dominance of mass transfer. The performance of the GDE eliminated MPL in the HT-PEMFC is higher than that of conventional GDE with MPL in this region because of the CL internal structural advantages, such as the interlaced macropore architecture based on the GDBL and the open CL inner surface, resulting in an enhanced gases diffusivity, by which the depletion of the reactant gases can be reduced, leading to an uncomplicated access of the reactants to the catalyst sites, consequently a low mass transfer loss. The current density of the GDE eliminated MPL reaches 0.29 A cm^{-2} at 0.6 V (Table 1), 32% higher than that of the conventional GDE (0.22 A cm^{-2}). The peak power density of the GDE eliminated MPL reached 0.54 W cm^{-2} at 0.36 V (Table 1). These results are comparable to the best ones yet reported for the HT-PEMFCs with similar Pt loading and operated using air [42]. In the case where the measurement was processed with H_2/O_2 (Fig. 5(b)), the performance of the MPL-free GDE was also better. Based on this result, the oxygen gains (ΔV) of the two electrodes were calculated to evaluate the difficulty of the transport of oxygen through their CLs, as shown in Fig. 5(c). High

oxygen gain means poor oxygen transport through the CL [43,44]. It is explicit that the MPL-free GDE possesses a lower oxygen gain, especially at higher current densities (> 1 A cm^{-2}). This means that oxygen can be more easily transported along the GDBL towards the catalyst sites, which is understood by the elimination of the MPL from the electrode and the open and interlaced macropore CL internal architecture originated from the GDBL.

Table 1. Structure and electrochemical properties of the GDEs.

Electrodes	Pt loading ($mg\ cm^{-2}$)	cumulative pore volume ($cm^3\ g^{-1}$)	Porosity	ECSA ($m^2\ g^{-1}$)	*Current density ($A\ cm^{-2}$)	Peak power density ($W\ cm^{-2}$)	$*R_{\Omega}$ ($\Omega\ cm^2$)	$*R_{ct}$ ($\Omega\ cm^2$)
MPL-free GDE	0.7	1.83	67.4%	31.14	0.29	0.54	0.34	0.43
Conventional GDE	0.7	1.34	51.3%	30.61	0.22	0.39	0.29	0.31

* Measured at 0.6 V with H_2/Air condition.

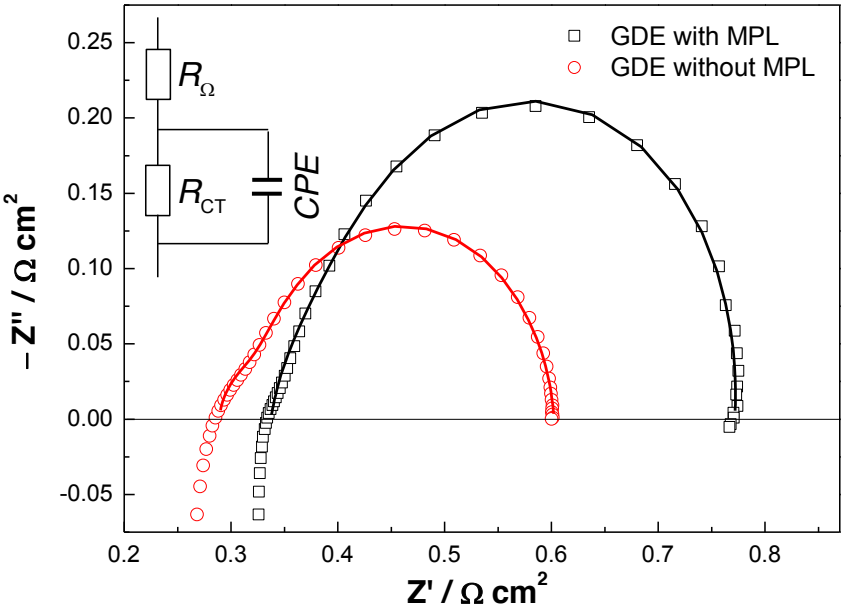

Fig. 6. *In situ* impedance curves of the single cell with different GDEs at cell voltage 0.6 V. Solid lines are fits obtained using the equivalent circuit.

The resistances of the two GDEs was determined in the single cell fixture at 0.6 V by *in situ* impedance measurements, as shown in Fig. 6. Their cell resistances (R_Ω) and charge transfer resistances (R_{ct}) were obtained by fitting the data with a Randels model equivalent circuit (see the insert of Fig. 6), which are shown in Table 1. It is explicitly that the elimination of MPL from the GDE effectively decreased the cell ohmic resistance from 0.34 Ω cm^2 to 0.29 Ω cm^2, suggesting an ample interfacial contact is still formed even with the uneven CL, which is documented by the cross-section image of this MEA showed in Fig. 7. A reduction of ~28% in charge transfer resistance can be also achieved (from 0.43 Ω cm^2 to 0.31 Ω cm^2) by eliminating MPL from the GDE, implying that the CL incorporating into the

interlaced macroporous GDBL could be more electrochemically active, leading to more efficient electrochemical process in the MPL-free electrodes.

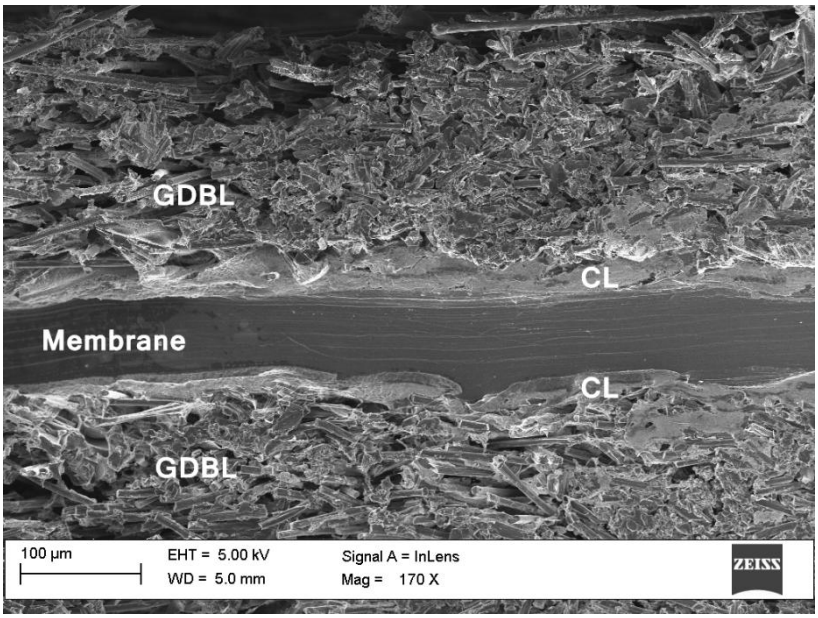

Fig. 7. Cross-section image of the MEA with the GDEs elimilated MPL.

3.3 Stability

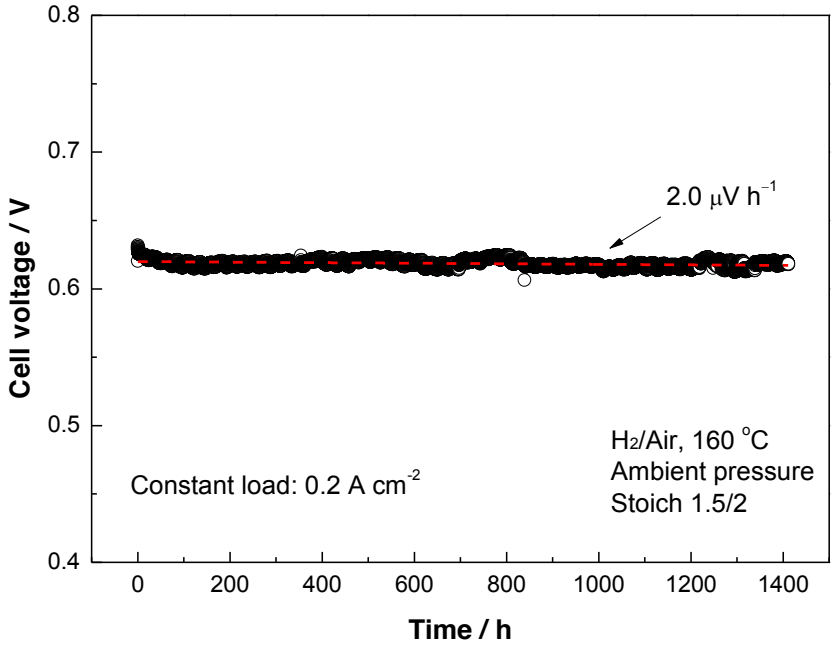

Fig. 8. Durability test of the MEA with the MPL-free GDEs.

A major concern for the MPL-free GDE operating in a PA-based HT-PEMFC system is its performance stability. Generally, the loss of acid from the PBI-based HT-PEMFC system is considered as a major mechanism for the HT-PEMFC performance degradation during short term operation [45]. The elimination of MPL may intensify the removal of PA from the MEA due to the reduced GDE thickness. To verify the stability of the MPL-free GDE, a primary durability test (after activation process) was performed by continuously operating the resultant MEA at 0.2 A cm^{-2}, as shown in Fig. 8. Surprisingly, the GDE shows excellent stability for more than 1400 hours operation: the voltage of the single cell is still around 0.62 V (only 2.2% decrease) without obvious drop after the durability test. Two reasons are considered for this result. First, the sintered PTFE-bonded CL is expected to be more

hydrophobic than a MPL due to the higher PTFE content (25 wt.% vs. 15 wt.%), which could repel any mobile PA from the membrane, thus a high PA doping level was maintained in the membrane. Furthermore, the well-distrusted PTFE network in the CL is highly hydrophobic, which can hold the impregnated PA, thereby the leaching of PA could be reduced and abundant triple-phase boundaries (TPBs) were also well maintained in the CLs [11]. Second, the elimination of MPL greatly decreased the amount of micro pores in the GDE, resulting in an inferior capillarity, which reduced the wicking of PA from the CL, thereby, the PA loss. Through a linear fitting on cell voltage data during the whole time period, the degradation rate obtained is around 2.0 $\mu V\ h^{-1}$, which is comparable to the best values (normally 2~10 $\mu V\ h^{-1}$) reported in other researchers' long-term durability tests [34,46], indicating the feasibility of the MPL-free GDE for real HT-PEMFC applications.

Conclusions and remarks

In summary, we demonstrated a simple way that eliminating MPL from GDE for use in HT-PEMFC to show high performance. By employing a higher PTFE content (~25 wt.%) in the GDBL, serious penetration of catalyst particles can be avoided, then maintaining a good catalyst utilization with a high catalyst loading (0.7 $mg_{Pt}\ cm^{-2}$). The catalyst were mainly deposited onto the stems and the junctions of the carbon fibers, forming a 3D interlaced micropore/macropore composited CL structure, leading to an improved effective porosity and minimized gas transport limitations.

The electrode showed a much higher performance than the conventional one, especially when air was used as an oxidant. Also, the electrode demonstrated excellent durability during 1400 h fuel cell operation, owing to its unique electrode architecture. Hence, our strategy of eliminating MPL from GDE is a simple way with promising performance and durability toward HT-PEMFCs.

The proposed approach also gives a new direction to design or modify GDBL for HT-PEMFCs. It is expected that the cell performance can be further improved by employing GDBLs with optimized properties (e.g. pore size), which could further increase the catalyst utilization and simultaneously maintain an efficient mass transport for this type of electrode. Moreover, with our MPL-free GDE, low Pt-wt% catalysts (e.g. 20 wt.%), which are normally with higher Pt utilizations, can be more widely used in HT-PEMFCs without the concern of an extremely high electrode thickness resulting from the use of high Pt loadings, thus holding the possibility of reducing the Pt loading for HT-PEMFCs.

Acknowledgements

We thank the financial support from National Natural Science Foundation of China (NSFC Project Nos. 21676126) and Hydrogen and Fuel Cell Technologies RDI Programme (HySA), funded by the Department of Science and Technology in South Africa (project KP1-S01).

References

[1] Q. Li, J.O. Jensen, R.F. Savinell, N.J. Bjerrum, Prog. Polym. Sci., 34 (2009) 449-477.

[2] S. Bose, T. Kuila, T.X.H. Nguyen, N.H. Kim, K.-t. Lau, J.H. Lee, Prog. Polym. Sci., 36 (2011) 813-843.

[3] E. Quartarone, P. Mustarelli, Energy Environ. Sci. , 5 (2012) 6436-6444.

[4] J. Lobato, P. Cañizares, M.A. Rodrigo, J.J. Linares, Appl. Catal. B, 91 (2009) 269-274.

[5] A. Orfanidi, M.K. Daletou, S.G. Neophytides, Appl. Catal. B, 106 (2011) 379-389.

[6] A. Stassi, I. Gatto, V. Baglio, E. Passalacqua, A.S. Aricò, Appl. Catal. B, 142–143 (2013) 15-24.

[7] S. Kaserer, K.M. Caldwell, D.E. Ramaker, C. Roth, J. Phys. Chem. C, 117 (2013) 6210-6217.

[8] I.E.L. Stephens, A.S. Bondarenko, U. Gronbjerg, J. Rossmeisl, I. Chorkendorff, Energy Environ. Sci. , 5 (2012) 6744-6762.

[9] H. Su, T.-C. Jao, S. Pasupathi, B.J. Bladergroen, V. Linkov, B.G. Pollet, J. Power Sources, 246 (2014) 63-67.

[10] H. Su, S. Pasupathi, B. Bladergroen, V. Linkov, B.G. Pollet, Int. J. Hydrogen Energy, 38 (2013) 11370-11378.

[11] H. Su, S. Pasupathi, B.J. Bladergroen, V. Linkov, B.G. Pollet, J. Power Sources, 242 (2013) 510-519.

[12] W. He, B. Wang, J.H. Dickerson, Nano Energy, 1 (2012) 828-832.

[13] J.H. Chun, D.H. Jo, S.G. Kim, S.H. Park, C.H. Lee, S.H. Kim, Renewable Energy, 48 (2012) 35-41.

[14] J.H. Chun, K.T. Park, D.H. Jo, J.Y. Lee, S.G. Kim, E.S. Lee, J.-Y. Jyoung, S.H. Kim, Int. J. Hydrogen Energy, 35 (2010) 11148-11153.

[15] J.H. Chun, K.T. Park, D.H. Jo, J.Y. Lee, S.G. Kim, S.H. Park, E.S. Lee, J.-Y.

Jyoung, S.H. Kim, Int. J. Hydrogen Energy, 36 (2011) 8422-8428.

[16] L. Cindrella, A.M. Kannan, J.F. Lin, K. Saminathan, Y. Ho, C.W. Lin, J. Wertz, J. Power Sources, 194 (2009) 146-160.

[17] Y. Ji, G. Luo, C.-Y. Wang, J. Electrochem. Soc., 157 (2010) B1753.

[18] T. Kim, S. Lee, H. Park, Int. J. Hydrogen Energy, 35 (2010) 8631-8643.

[19] S. Latorrata, P.G. Stampino, E. Amici, R. Pelosato, C. Cristiani, G. Dotelli, Solid State Ionics, 216 (2012) 73-77.

[20] M. Maidhily, N. Rajalakshmi, K.S. Dhathathreyan, Int. J. Hydrogen Energy, 36 (2011) 12352-12360.

[21] S. Park, J.-W. Lee, B.N. Popov, J. Power Sources, 163 (2006) 357-363.

[22] S. Park, J.-W. Lee, B.N. Popov, J. Power Sources, 177 (2008) 457-463.

[23] U. Pasaogullari, C.-Y. Wang, Electrochim. Acta, 49 (2004) 4359-4369.

[24] R.P. Ramasamy, E.C. Kumbur, M.M. Mench, W. Liu, D. Moore, M. Murthy, Int. J. Hydrogen Energy, 33 (2008) 3351-3367.

[25] H. Tang, S. Wang, M. Pan, R. Yuan, J. Power Sources, 166 (2007) 41-46.

[26] X. Wang, H. Zhang, J. Zhang, H. Xu, X. Zhu, J. Chen, B. Yi, J. Power Sources, 162 (2006) 474-479.

[27] X.L. Wang, H.M. Zhang, J.L. Zhang, H.F. Xu, Z.Q. Tian, J. Chen, H.X. Zhong, Y.M. Liang, B.L. Yi, Electrochim. Acta, 51 (2006) 4909-4915.

[28] F.-B. Weng, C.-Y. Hsu, M.-C. Su, Int. J. Hydrogen Energy, 36 (2011) 13708-13714.

[29] R. Wu, X. Zhu, Q. Liao, H. Wang, Y.-d. Ding, J. Li, D.-d. Ye, Int. J. Hydrogen Energy, 35 (2010) 7588-7593.

[30] J. Lobato, P. Cañizares, M.A. Rodrigo, C. Ruiz-López, J.J. Linares, J. Appl. Electrochem., 38 (2008) 793-802.

[31] J. Lobato, P. Canizares, M.A. Rodrigo, D. Ubeda, F.J. Pinar, J.J. Linares, Fuel Cells, 10 (2010) 770-777.

[32] O.E. Kongstein, T. Berning, B. Børresen, F. Seland, R. Tunold, Energy, 32 (2007) 418-422.

[33] F. Seland, T. Berning, B. Børresen, R. Tunold, J. Power Sources, 160 (2006)

27-36.

[34] T.J. Schmidt, J. Baurmeister, J. Power Sources, 176 (2008) 428-434.

[35] K.L. Hsueh, E. Gonzalez, S. Srinivasan, D.T. Chin, J. Electrochem. Soc., 131 (1984) 823-828.

[36] K. Holst-Olesen, M. Nesselberger, M. Perchthaler, V. Hacker, M. Arenz, J. Power Sources, 272 (2014) 1072-1077.

[37] H. Su, C. Felix, O. Barron, P. Bujlo, B. Bladergroen, B. Pollet, S. Pasupathi, Electrocatalysis, 5 (2014) 361-371.

[38] B. Millington, V. Whipple, B.G. Pollet, Journal of Power Sources, 196 (2011) 8500-8508.

[39] M. Uchida, Y. Aoyama, N. Eda, A. Ohta, J. Electrochem. Soc., 142 (1995) 4143.

[40] O.H. Kim, Y.H. Cho, S.H. Kang, H.Y. Park, M. Kim, J.W. Lim, D.Y. Chung, M.J. Lee, H. Choe, Y.E. Sung, Nature Communications, 4 (2013) 2473.

[41] H.-K. Lee, J.-H. Park, D.-Y. Kim, T.-H. Lee, J. Power Sources, 131 (2004) 200-206.

[42] J. Zhang, Y. Tang, C. Song, J. Zhang, J. Power Sources, 172 (2007) 163-171.

[43] Y.G. Yoon, G.G. Park, T.H. Yang, J.N. Han, W.Y. Lee, C.S. Kim, Int. J. Hydrogen Energy, 28 (2003) 657-662.

[44] M. Prasanna, H.Y. Ha, E.A. Cho, S.A. Hong, I.H. Oh, J. Power Sources, 137 (2004) 1-8.

[45] S. Yu, L. Xiao, B.C. Benicewicz, Fuel Cells, 8 (2008) 165-174.

[46] Y. Oono, A. Sounai, M. Hori, J. Power Sources, 241 (2013) 87-93.

Table 1

Table 1. Structures and electrochemical properties of the electrodes.

Electrodes	Pt loading ($mg\ cm^{-2}$)	cumulative pore volume ($cm^3\ g^{-1}$)	Porosity	ECSA ($m^2\ g^{-1}$)	*Current density ($A\ cm^{-2}$)	Peak power density ($W\ cm^{-2}$)	$*R_{\Omega}$ ($\Omega\ cm^2$)	$*R_{ct}$ ($\Omega\ cm^2$)
MPL-free GDE	0.7	1.83	67.4%	31.14	0.29	0.54	0.34	0.43
Conventional GDE	0.7	1.34	51.3%	30.61	0.22	0.39	0.29	0.31

* Measured at 0.6 V with H_2/Air condition.

Figure 1

Click here to download Figure(s) - provide separately in addition to within the manuscript file: Fig1.docx

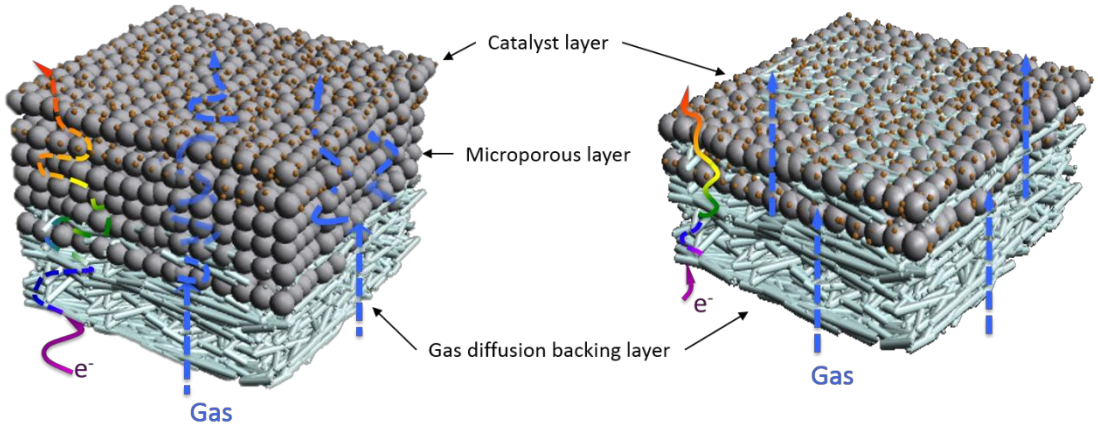

(a) (b)

Figure 3

Click here to download Figure(s) - provide separately in addition to within the manuscript file: Fig3.docx

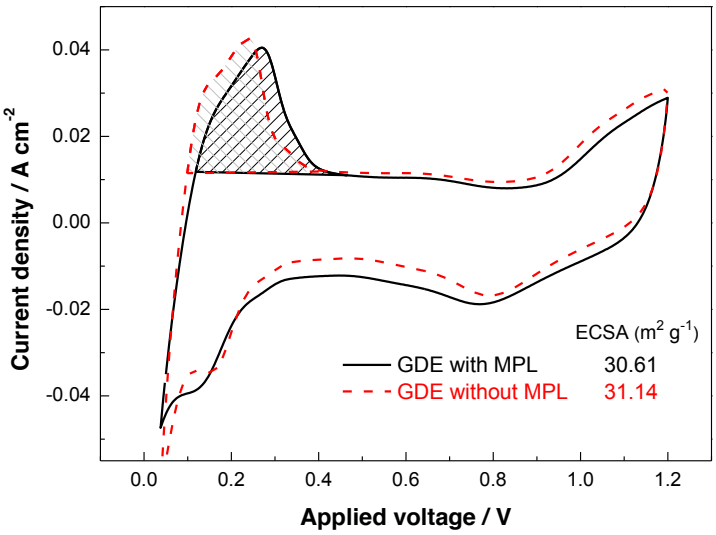

Figure 4

Click here to download Figure(s) - provide separately in addition to within the manuscript file: Fig4.docx

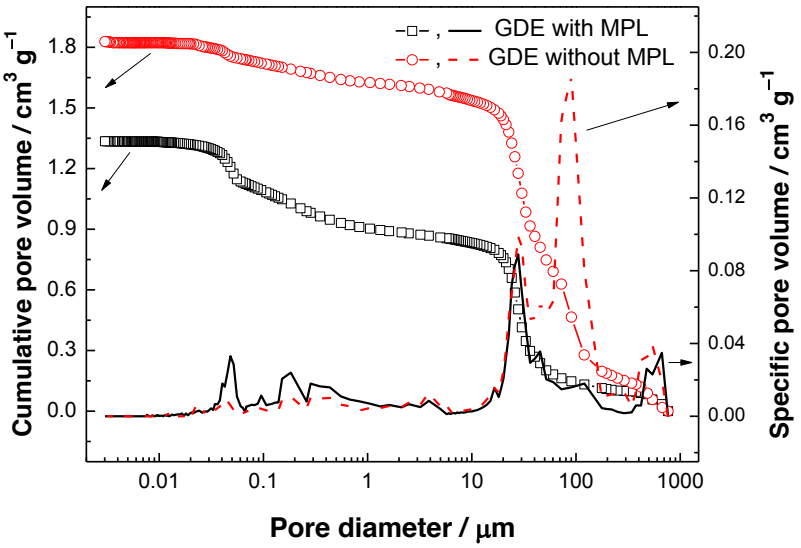

Figure 5

Click here to download Figure(s) - provide separately in addition to within the manuscript file: Fig5.docx

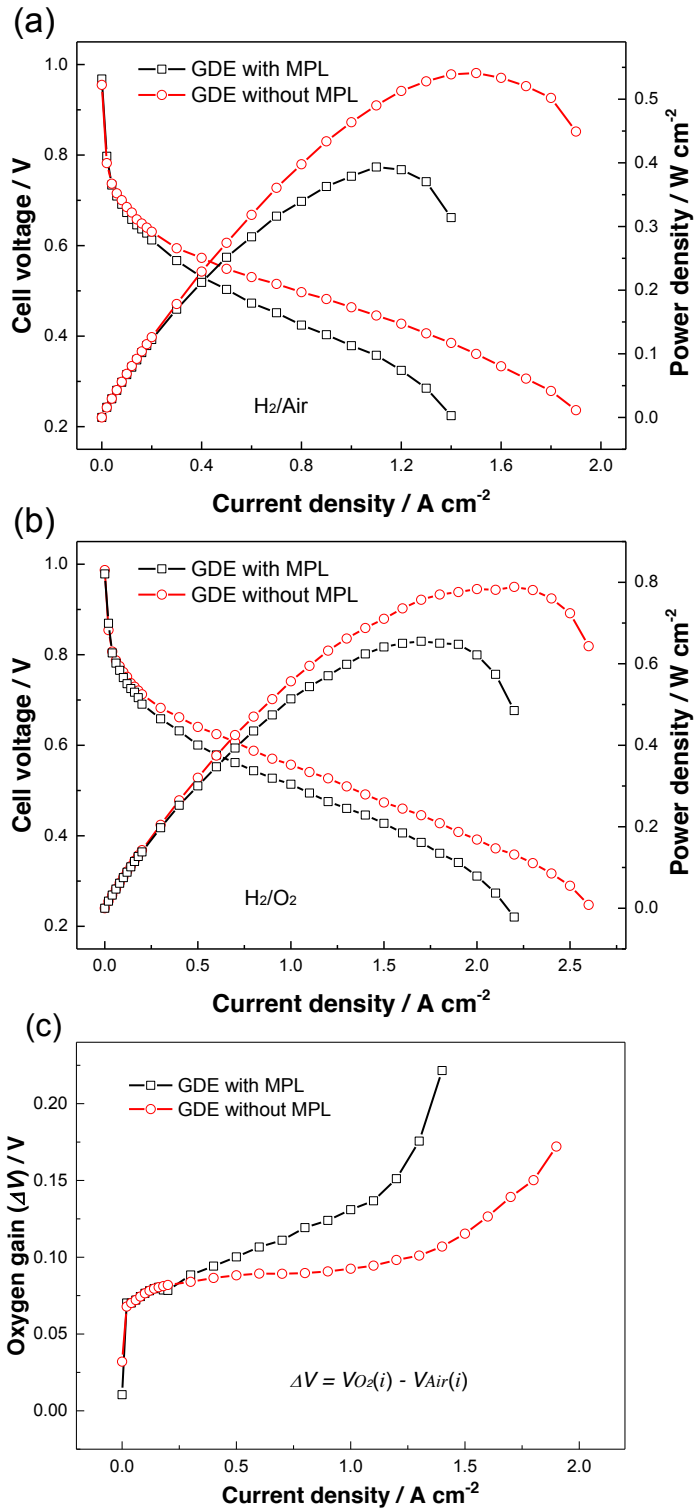

Figure 6

Click here to download Figure(s) - provide separately in addition to within the manuscript file: Fig6.docx

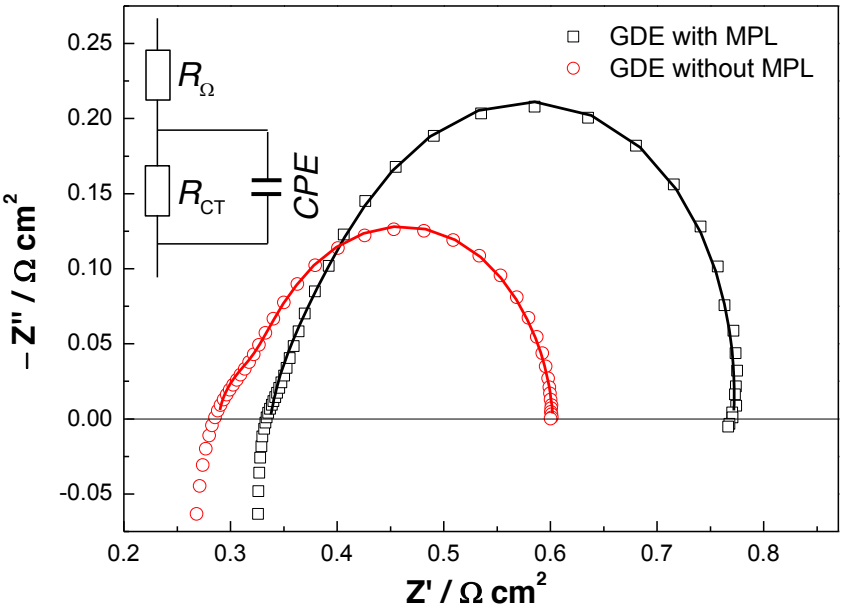

Figure 7

Click here to download Figure(s) - provide separately in addition to within the manuscript file: Fig7.docx

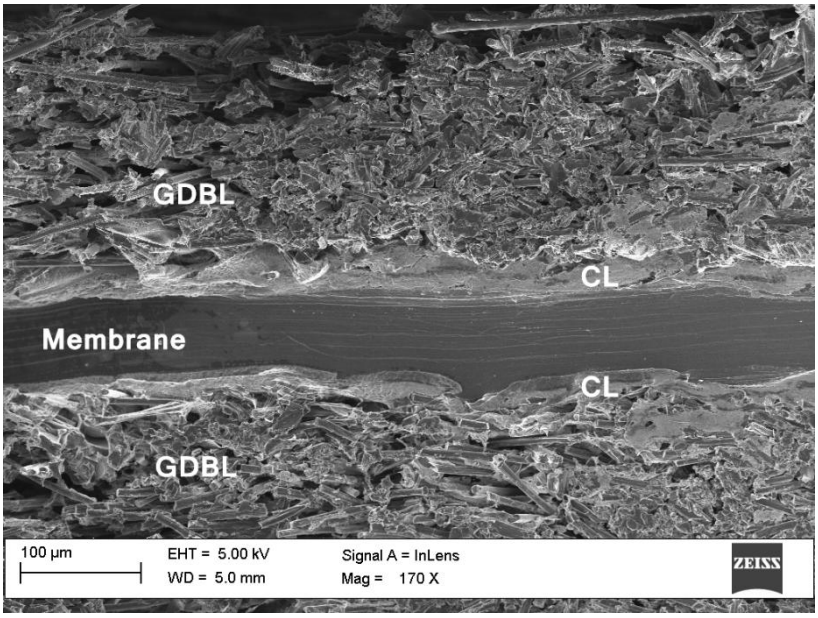

Figure 8

Click here to download Figure(s) - provide separately in addition to within the manuscript file: Fig8.docx

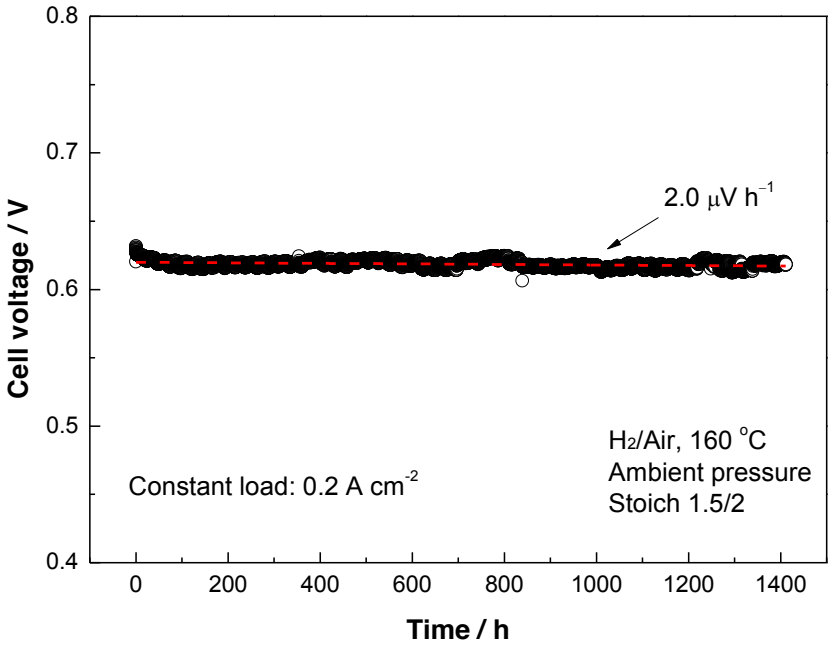

Figure 2

Click here to download Figure(s) - provide separately in addition to within the manuscript file: Fig2.docx

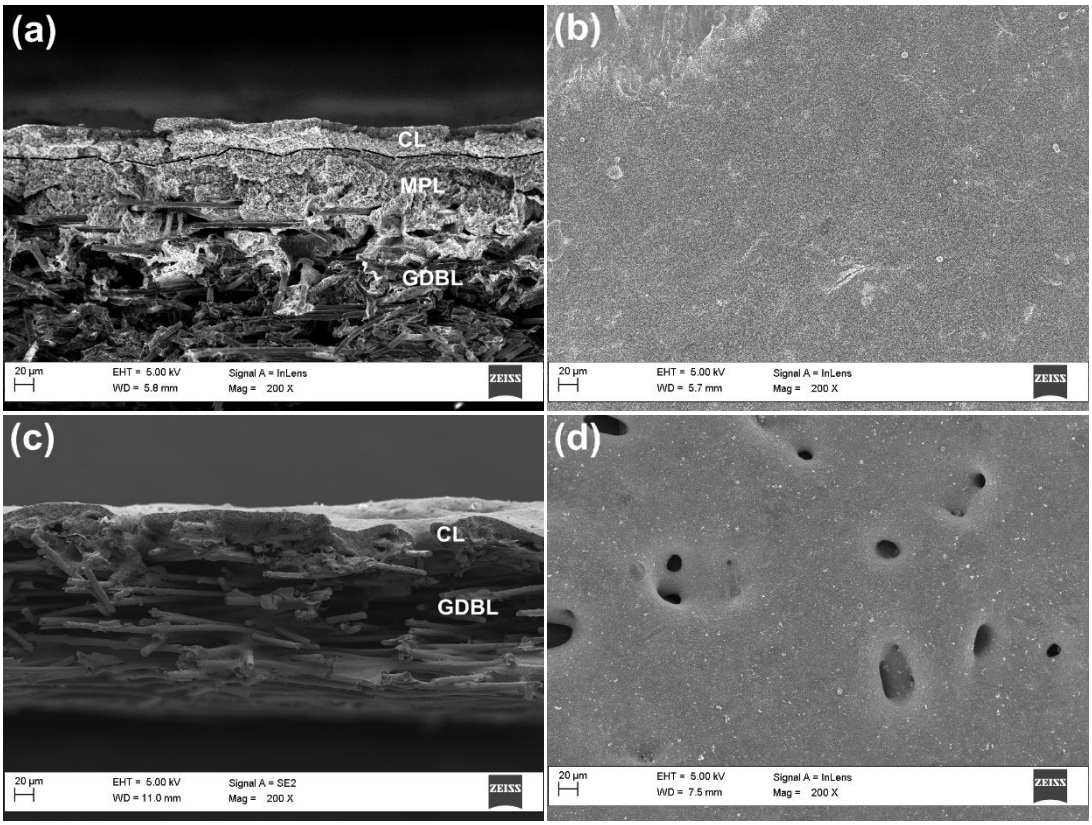

Figure Caption:

Fig. 1. Conceptual diagrams of the conventional GDE with MPL (a) and the GDE eliminated MPL (b).

Fig. 2. SEM images of the GDE with MPL (a, b) and the GDE without MPL (c, d) to show their cross-sections and surface morphologies.

Fig. 3. Cyclic voltammograms of the MEAs with the different GDEs.

Fig. 4. Pore size distribution of the two GDEs.

Fig. 5. Polarization curves and power density curves of the single cell using GDEs with/without MPL, operated at 160 oC and ambient pressure, with (a) 1.5/2 stoichiometry of H2/Air, (b) 1.5/2 stoichiometry of H2/O2; and (c) Oxygen gain.

Fig. 6. *In situ* impedance curves of the single cell with different GDEs at cell voltage 0.6 V. Solid lines are fits obtained using the equivalent circuit.

Fig. 7. Cross-section image of the MEA with the GDEs elimilated MPL

Fig. 8. Durability test of the MEA with the MPL-free GDEs.

Table Caption:

Table 1. Structures and electrochemical properties of the electrodes.